

Iron-Molybdenum-oxo complexes as initiators for olefin autoxidation with O₂ - Electronic Supporting Information

Jan P. Falkenhagen,^a Christian Limberg,^{*a} Serhiy Demeshko,^b Sebastian Horn,^c Michael Haumann,^c Beatrice Braun,^a and Stefan Mebs^a

^a Institut für Chemie, Humboldt-Universität zu Berlin, Brook-Taylor-Straße 2, 12489 Berlin, Germany.
Fax: +49 30 2093 6966;
Tel: +49 30 2093 7382;
E-mail: christian.limberg@chemie.hu-berlin.de

^b Institut für Anorganische Chemie, Georg-August-Universität Göttingen, Tammannstraße 4, 37077 Göttingen, Germany.

^c Fachbereich Physik, Freie Universität Berlin, 14195 Berlin, Germany.

Contents

1 Cyclooctene Epoxidation	3
2 Crystal structure determination	5
2.1 Molecular structure of $[(\text{TPA})\text{Fe}_2(\mu-\text{O})(\mu-\text{MoO}_4)](\text{OTf})_2$ (2)	5
2.2 Molecular structure of $[(\text{TPA})\text{Zn}(\text{Cp}^*\text{MoO}_3)](\text{OTf})(\text{MeCN})_2$ (3 ·(MeCN) ₂)	6
2.3 Molecular structure of $[(\text{TPA})\text{Fe}(\mu-\text{MoO}_4)]_2$ (6 ·(MeCN) ₂)	7
2.4 Crystal data and experimental parameters	8
3 NMR spectroscopy	9
3.1 ¹ H-NMR spectrum of $[(\text{TPA})\text{Fe}(\mu-\text{Cp}^*\text{MoO}_3)]_2(\text{OTf})_2$ (1)	9
3.2 ¹ H-NMR spectrum of $[(\text{TPA})\text{Co}(\text{Cp}^*\text{MoO}_3)](\text{OTf})$ (4)	11
3.3 <i>T</i> ₁ measurements	13
4 XA Spectroscopy	15
4.1 Materials and Methods	15
4.2 Results	15
5 UV/VIS Spectroscopy	17
5.1 UV/VIS spectrum of $[(\text{TPA})\text{Fe}(\mu-\text{Cp}^*\text{MoO}_3)]_2(\text{OTf})_2$ (1)	17
5.2 UV/VIS spectrum of $[(\text{TPA})\text{Fe}_2(\mu-\text{O})(\mu-\text{MoO}_4)](\text{OTf})_2$ (2)	18
5.3 UV/VIS spectrum of $[(\text{TPA})\text{Zn}(\text{Cp}^*\text{MoO}_3)]\text{OTf}$ (3)	19
5.4 UV/VIS spectrum of $[(\text{TPA})\text{Co}(\text{Cp}^*\text{MoO}_3)](\text{OTf})$ (4)	20
5.5 UV/VIS spectrum of $[(\text{TPA})\text{Co}_2(\mu-\text{Mo}_2\text{O}_8)](\text{OTf})_2$ (5)	21
5.6 UV/VIS spectrum of $[(\text{TPA})\text{Fe}(\mu-\text{MoO}_4)]_2$ (6)	22
6 Mößbauer Spectroscopy of $[(\text{TPA})\text{Fe}(\mu-\text{Cp}^*\text{MoO}_3)]_2(\text{OTf})_2$ (1)	23

1 Cyclooctene Epoxidation

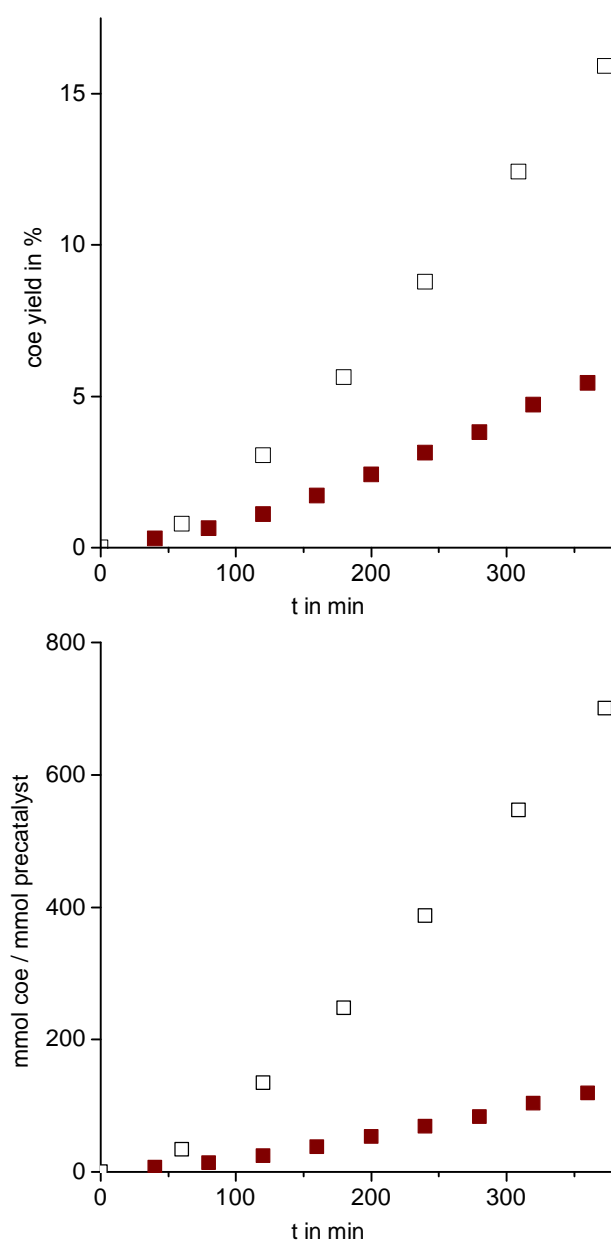


Figure S1: Yield of cyclooctene autoxidation vs time at 80 °C. Acetonitrile (12 mL), O₂ (1.2 bar), diphenyl ether (70 μmol): □ 3.5 μmol **1** and 15.4 mmol cyclooctene, ■ 3.5 μmol **1** and 7.7 mmol cyclooctene.

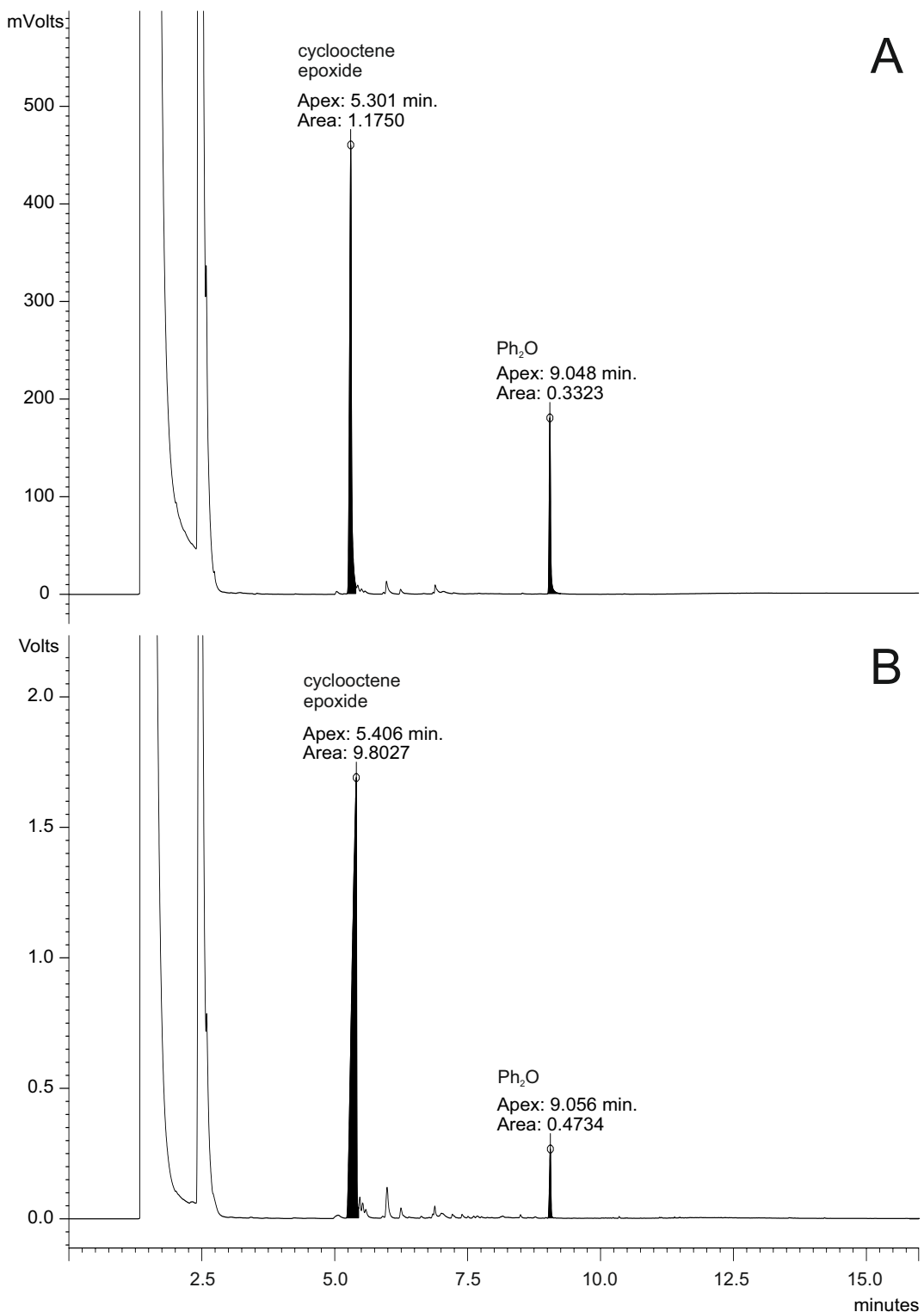


Figure S2: GC chart of the autoxidation experiments: Acetonitrile (12 mL), O₂ (1.2 bar), diphenyl ether (70 μ mol), 3.5 μ mol **1** and (A) 7.7 mmol cyclooctene after 6 h; (B) 15.4 mmol cyclooctene after 6.25 h.

2 Crystal structure determination

2.1 Molecular structure of $[(\text{TPA})\text{Fe}_2(\mu-\text{O})(\mu-\text{MoO}_4)](\text{OTf})_2$ (2).

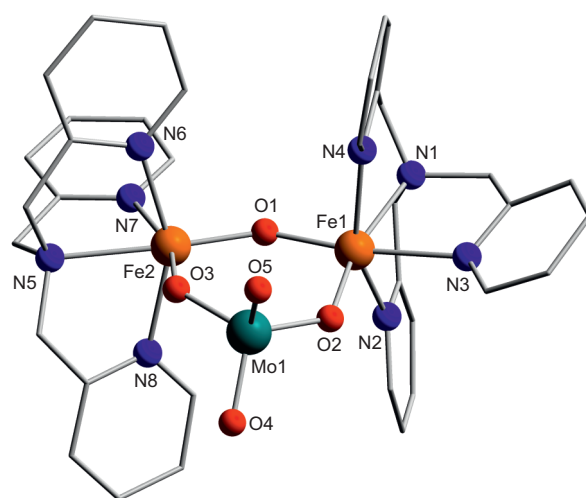


Figure S3: Molecular structure of the cation of $[(\text{TPA})\text{Fe}_2(\mu-\text{O})(\mu-\text{MoO}_4)](\text{OTf})_2$ (**2**) in the single crystal unit cell. Hydrogen atoms, triflate anions and co-crystallised solvent molecules have been omitted for clarity. Selected bond lengths (in Å) and angles (in °). Fe1–O1 1.8254(13), Fe2–O1 1.7965(13), Fe1–O2 1.9248(14), Fe2–O3 1.9678(14), Mo1–O2 1.8203(13), Mo1–O3 1.7988(14), Mo1–O4 1.7235(15), Mo1–O5 1.7242(15), Fe2–O1–Fe1 141.56(8), Mo1–O2–Fe1 132.67(8), Mo1–O3–Fe2 131.89(7), O1–Fe1–O2 99.62(6), O1–Fe2–O3 101.05(6), O4–Mo1–O5 108.47(8), O4–Mo1–O3 112.01(7), O5–Mo1–O3 107.92(7), O4–Mo1–O2 111.78(7), O5–Mo1–O2 109.98(7), O3–Mo1–O2 106.62(6).

2.2 Molecular structure of [(TPA) $\text{Zn}(\text{Cp}^*\text{MoO}_3)$](OTf)(MeCN)₂ (3·(MeCN)₂).

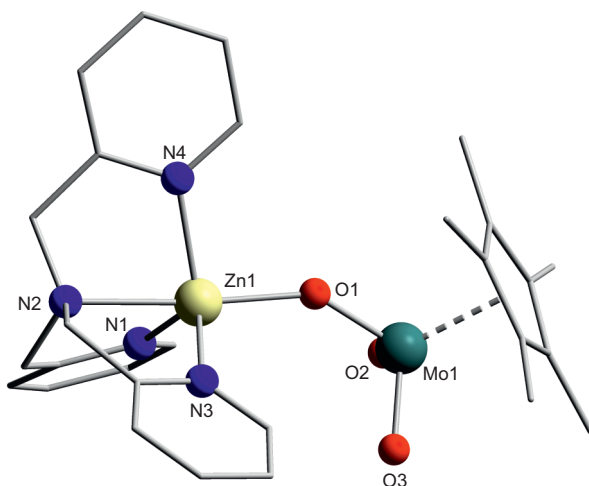


Figure S4: Molecular structure of the cation of $[(\text{TPA})\text{Zn}(\text{Cp}^*\text{MoO}_3)](\text{OTf})(\text{MeCN})_2$ $\mathbf{3}\cdot(\text{MeCN})_2$ in the single crystal unit cell. Hydrogen atoms, triflate anions and co-crystallised solvent molecules have been omitted for clarity. Selected bond lengths (in Å) and angles (in °). Zn1–O1 1.966(6), O1–Mo1 1.795(5), Mo1=O2 1.723(5), Mo1=O3 1.728(6), Mo1–C_g 2.123(4), Co1–O1–Mo1 145.2(3), O1–Mo1–O2 106.5(2), O2–Mo1–O3 105.5(3), O3–Mo1–O1 106.3(3).

2.3 Molecular structure of $[(\text{TPA})\text{Fe}(\mu-\text{MoO}_4)]_2 (\mathbf{6}\cdot(\text{MeCN})_2)$.

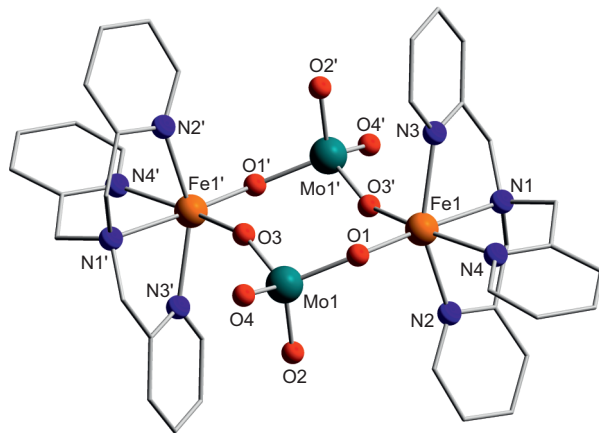


Figure S5: Molecular structure of the cation of $[(\text{TPA})\text{Fe}(\mu-\text{MoO}_4)]_2(\text{MeCN})_2$ (**6** \cdot (MeCN) $_2$) in the single crystal unit cell. Hydrogen atoms and co-crystallised solvent molecules have been omitted for clarity. Selected bond lengths (in Å) and angles (in °). Fe1–O1 1.961(3), Fe1–O3 2.085(3), Mo1–O2 1.731(3), Mo1–O4 1.737(3), Mo1–O3 1.766(3), Mo1–O1 1.821(3), Mo1–O1–Fe1 128.36(14), Mo1–O3–Fe1 154.31(15), O1–Fe1–O3 98.23(11), O2–Mo1–O4 109.01(15), O2–Mo1–O3 110.39(14), O4–Mo1–O3 107.47(13), O2–Mo1–O1 109.31(13), O4–Mo1–O1 108.98(13), O3–Mo1–O1 111.62(12).

2.4 Crystal data and experimental parameters

Table S1: Crystal data and experimental parameters for the crystal structure analysis of **3**·(MeCN)₂, **2** and **6**·(MeCN)₂.

compound	3 ·(MeCN) ₂	2	6 ·(MeCN) ₂
formula	C ₃₃ H ₃₉ F ₃ Mo N ₆ O ₆ SZn	C ₃₈ H ₃₆ F ₆ Fe ₂ Mo N ₈ O ₁₁ S ₂	C ₄₀ H ₄₂ Fe ₂ Mo ₂ N ₁₀ O ₈
formula weight / (g·mol ⁻¹)	866.07	1166.51	1094.42
Crystal system	Monoclinic	Triclinic	Triclinic
Space group	P2 ₁ /c	P $\bar{1}$	P $\bar{1}$
a / Å	19.2094(6)	10.0539(4)	8.2347(4)
b / Å	14.0319(3)	14.1854(5)	10.7794(6)
c / Å	14.4470(4)	16.1221(7)	11.9562(6)
α / °	90	84.611(3)	88.958(4)
β / °	106.646(2)	78.110(3)	86.074(4)
γ / °	90	78.873(3)	89.140(5)
V / Å ³	3730.92(17)	2204.17(15)	1058.53(9)
Z	4	2	1
Density / (g·cm ⁻³)	1.542	1.758	1.717
μ (Mo-K α) / mm ⁻¹	1.100	1.118	1.315
F(000)	1768	1176	552
Θ range / °	2.83–25.00	3.27–29.57	3.42–26.00
Reflections collected	65943	33490	21217
Independent reflections	6568	12261	4154
completeness to Θ	0.998	0.993	1.000
R(int)	0.1160	0.0361	0.0899
GoF on F^2	1.081	0.988	0.904
R_1 [I>2σ(I)]	0.0863	0.0313	0.0373
wR ₂ [I>2σ(I)]	0.2070	0.0722	0.0880
R_1 (all data)	0.1027	0.0451	0.0477
wR ₂ (all data)	0.2174	0.0773	0.0895
$\Delta\rho_{max}/\Delta\rho_{min}$ / (e·Å ⁻³)	1.916/-1.232	0.66/-1.30	0.754/-1.656
CCDC	936996	937040	936999

3 NMR spectroscopy

3.1 ^1H -NMR spectrum of $[(\text{TPA})\text{Fe}(\mu-\text{Cp}^*\text{MoO}_3)]_2(\text{OTf})_2$ (**1**)

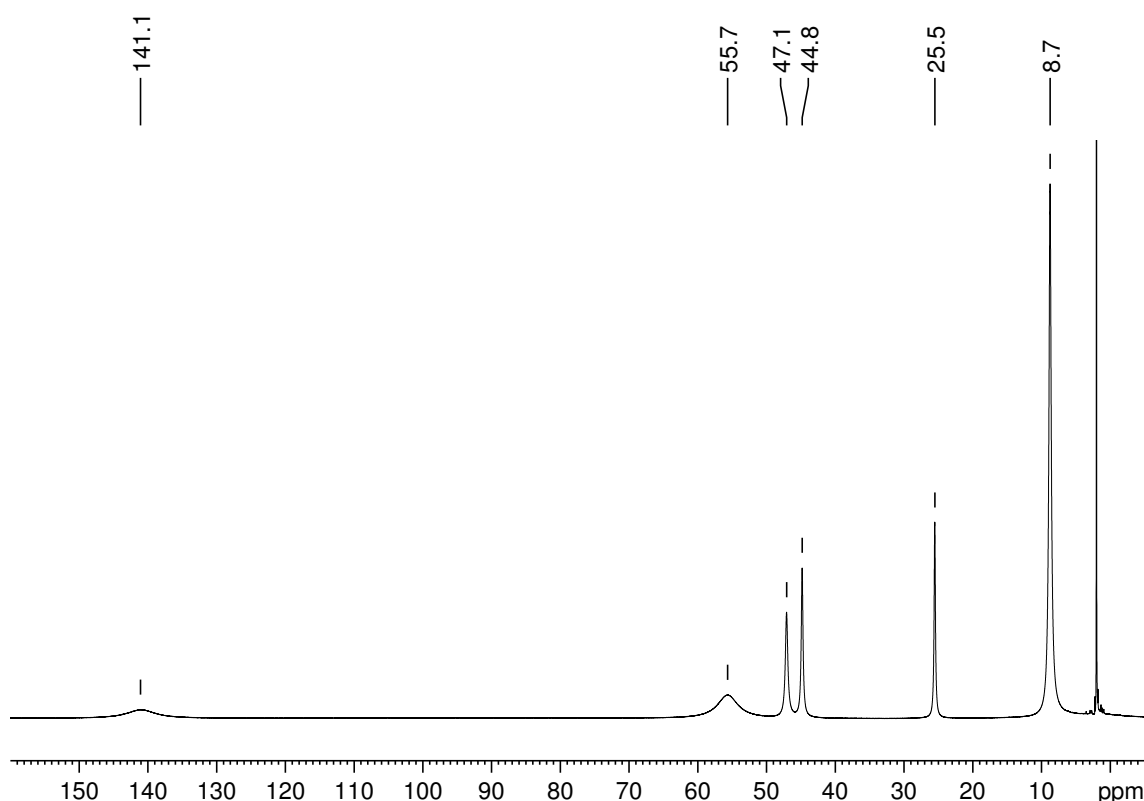


Figure S6: ^1H -NMR spectrum of **1** in acetonitrile- d_3 at 300.1 MHz and 300 K.

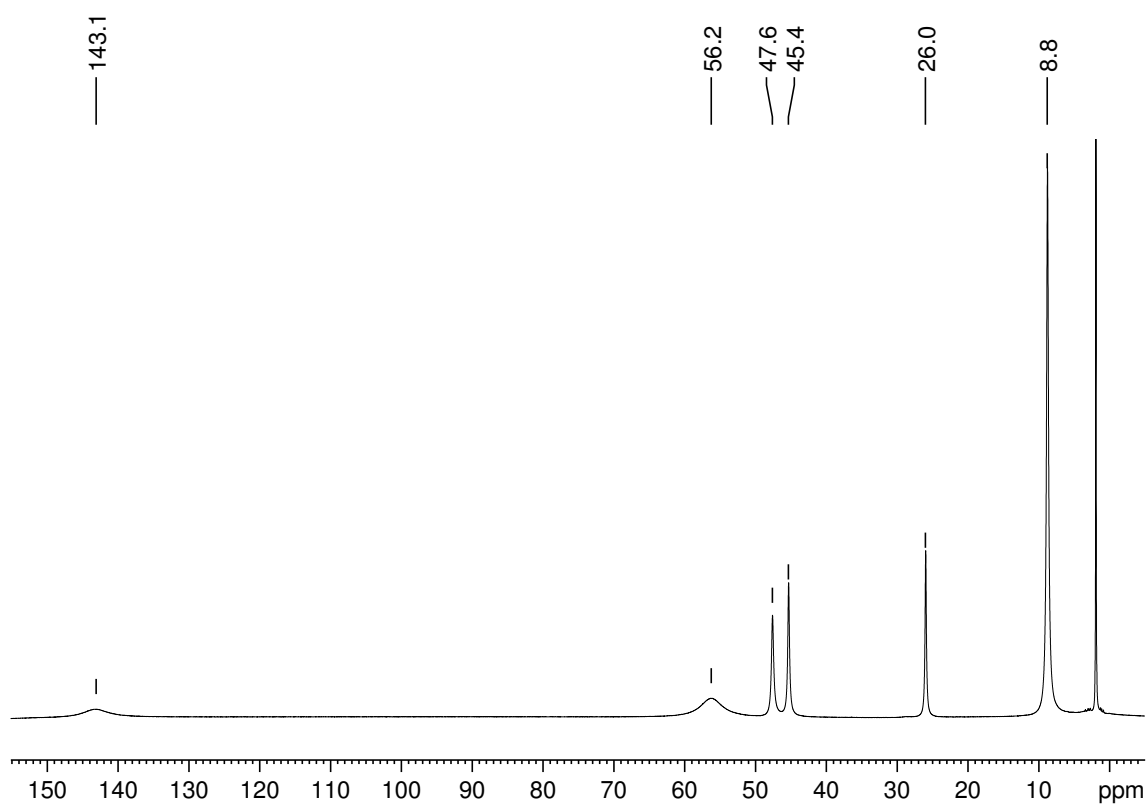


Figure S7: ¹H-NMR spectrum of **1** in acetonitrile-d₃ at 500.1 MHz and 296 K.

3.2 ^1H -NMR spectrum of $[(\text{TPA})\text{Co}(\text{Cp}^*\text{MoO}_3)](\text{OTf})$ (4)

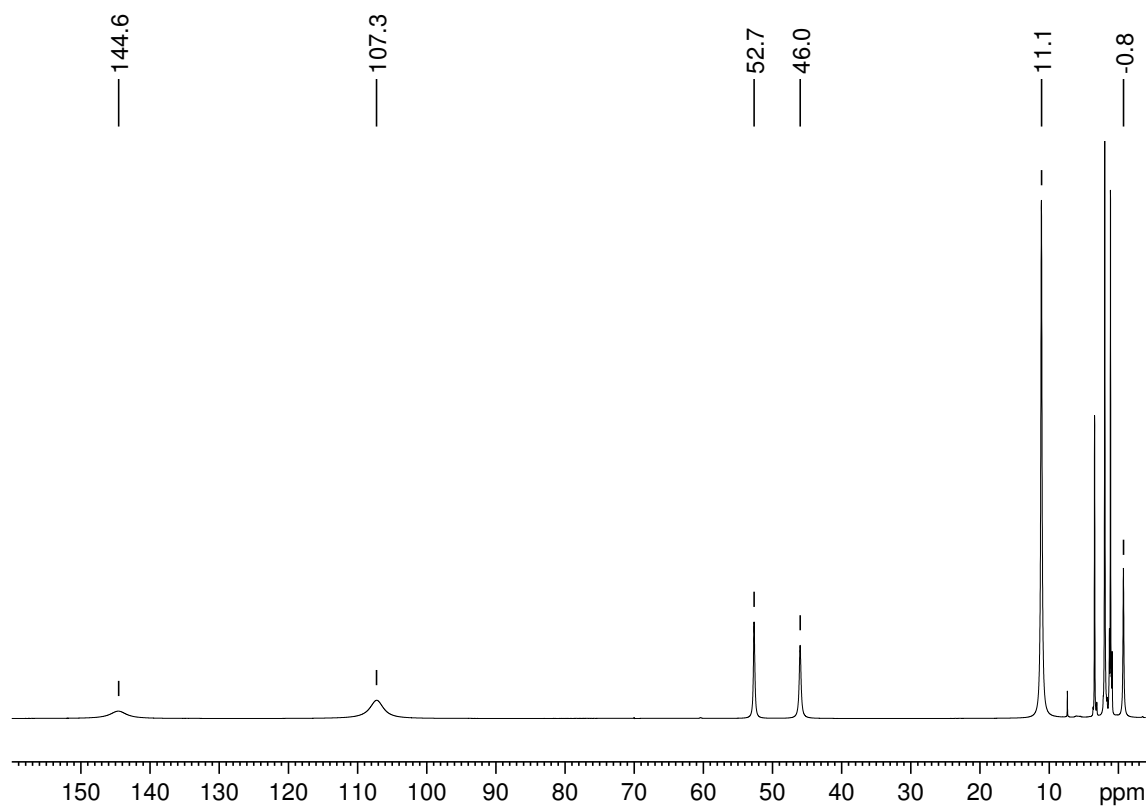


Figure S8: ^1H -NMR spectrum of **4** in acetonitrile- d_3 at 300.1 MHz and 296 K. The impurity signals in the diamagnetic region are caused by residual diethyl ether, as crystals were used for this experiment.

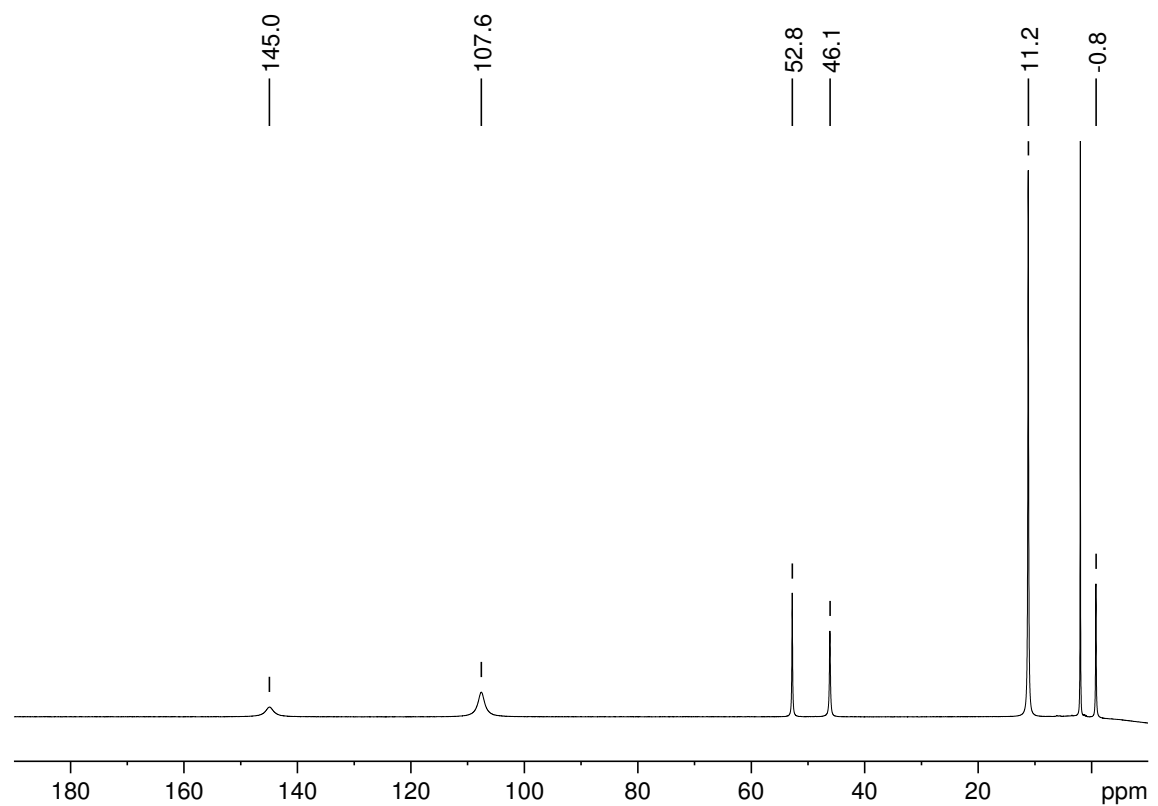


Figure S9: ¹H-NMR spectrum of **4** in acetonitrile-d₃ at 500.1 MHz and 295 K.

3.3 T_1 measurements

Measurements to obtain nonselective proton longitudinal relaxation times (T_1) were performed using a standard inversion recovery experiment with a $180^\circ\text{-}\tau\text{-}90^\circ\text{-AQ}$ pulse sequence. To secure the validity of the results, for each sample multiple experiments with different transmitter frequency offsets were carried out. The Bruker Topspin T_1/T_2 module was used to obtain T_1 values in a nonlinear fitting procedure. For paramagnetic complexes T_1 values can be correlated to the distances of the respective protons from the metal centre using the Solomon equation.¹

$$T_{1M}^{-1} = C[S(S+1)]r_{MH}^{-6}f(\tau_c, \omega) \quad (\text{S1})$$

where C represents a combination of physical constants and $f(\tau_c, \omega)$ is the correlation function. Adapting this equation for two non-coupling metal centres leads to:

$$T_{1M\text{exp}}^{-1} = T_{1M}^{-1} + T_{1M'}^{-1} \quad (\text{S2})$$

$$T_{1M\text{exp}}^{-1} = C[S(S+1)](r_{MH}^{-6} + r_{M'H}^{-6})f(\tau_c, \omega) \quad (\text{S3})$$

$$T_{1M\text{calc}}^{-1} = T_{1M\text{ref}}^{-1}(r_{MH}^{-6} + r_{M'H}^{-6})/(r_{MH}^{-6} + r_{M'H}^{-6})_{\text{ref}} \quad (\text{S4})$$

which was used to calculate theoretical relaxation times for pyridyl protons interacting (distances $r_{MH}/r_{M'H}$ were taken from the molecular structures in the single crystals) with one ($T_{1\text{calc},M}$) or two ($T_{1\text{calc},M,M'}$) metal centres against the relaxation time $T_{1M\text{ref}}$ of a reference signal.

Table S2: NMR Parameters, experimental and calculated Results of the proton longitudinal relaxation time (T_1) measurements of **1** in acetonitrile-d₃ at 296 K and 500.1 MHz.

	δ , ppm	int	fwhm, Hz	r_{MH} , Å	$r_{M'H}$, Å	$T_{1\text{exp}}$, ms	$T_{1\text{calc},M}$, ms	$T_{1\text{calc},M,M'}$, ms
α -H	143.1	4	2000	3.24	6.28	0.2	0.2	0.3
CH ₂	56.2	10	1700	3.61	7.40	0.4	0.5	0.5
β' -H	47.6	6	170	5.03	8.67	3.1	3.4	3.6
β -H ^{ref}	45.4	6	125	5.20	8.06	4.2	4.2	4.2
γ -H	26.0	6	95	5.88	9.11	10.4	8.8	8.8
CH ₃	8.8	30	145			3.7		

$T_{1M,\text{calc}}$ have been calculated using the Solomon equation^{1,2} employing the pyridyl β protons as the reference for T_1 . Averaged proton-iron distances were extracted from the molecular structure of **1**. For comparison values accounting for the influence of the distant iron(II) centre have been calculated showing negligible effect on the calculated $T_{1MM'\text{calc}}$ values.

Table S3: NMR Parameters, experimental and calculated Results of the proton longitudinal relaxation time (T_1) measurements of **4** in acetonitrile-d₃ at 296 K and 500.1 MHz.

	δ , ppm	int	fw hm, Hz	r _{MH} , Å	$T_{1\text{exp}}$, ms	$T_{1\text{calc,M}}$, ms
α -H	144.3	3	800	3.06	0.4	0.4
CH ₂	107.1	6	690	3.51	0.7	0.8
β -H	52.5	3	56	5.04	14.3	7.1
β -H ^{ref}	45.9	3	83	4.97	6.5	6.5
CH ₃	11.1	15	55		7.8	
γ -H	-0.8	3	43	5.80	22.5	16.5

$T_{1M,\text{calc}}$ have been calculated using the Solomon equation^{1,2} employing the pyridyl β protons as the internal reference for T_1 . Averaged proton-cobalt distances were extracted from the molecular structure of **4**.

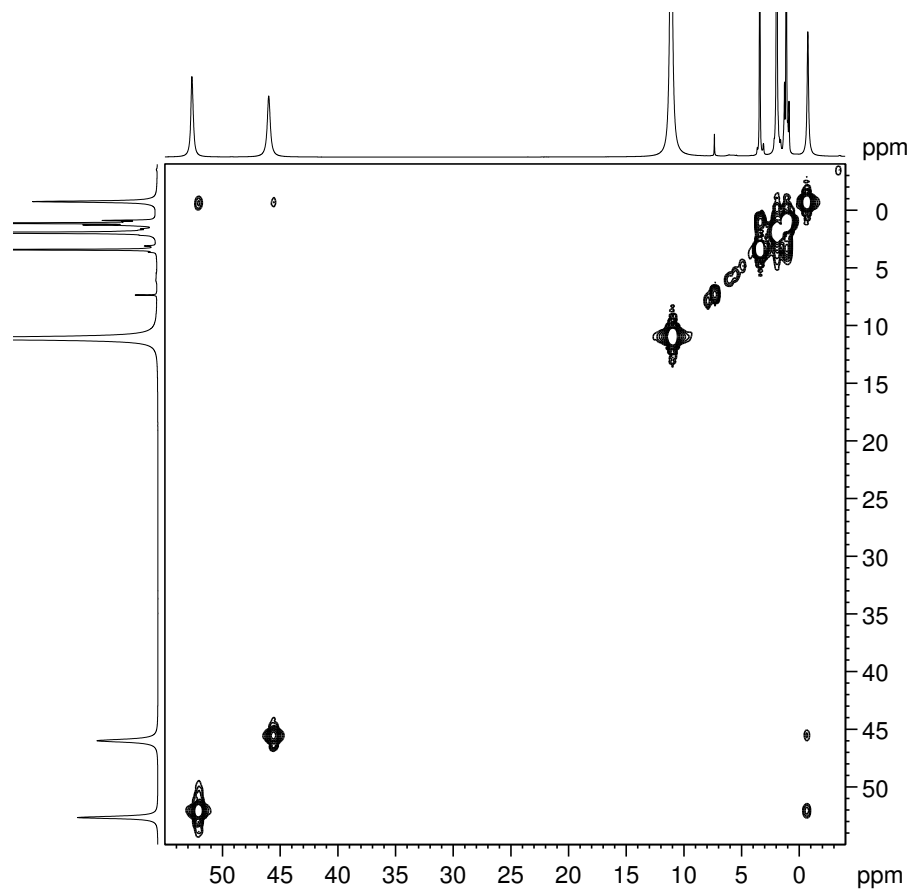


Figure S10: ^1H -COSY-DQF nmr spectrum of **4** in acetonitrile-d₃ at 25 °C and 300.1 MHz. Unshifted squared sine window functions were applied in F1/F2. No symmetrization has been performed. The impurity signals in the diamagnetic region are caused by residual diethyl ether, as crystals were used for this experiment.

Table S4: EXAFS fit parameters.^a

Mo–O			Mo–C			Mo–Fe		
	N per Mo	R /Å	2σ ² /Å ²		N per Mo	R /Å	2σ ² /Å ²	R _F /%
1	1	1.74	3		5	2.42	5	19.4
	2	1.77	2		5	2.92	23	2
1/O₂	2	1.70	3				1	3.29
	2	1.93	10				1	3.44

^a N, coordination number; R, interatomic distance; 2σ², Debye-Waller factor ×10³; R_F, error sum. Coordination numbers were fixed to integer values in the fit procedure. E₀ was 20015±1 eV, S₀² was 0.8.

4 XA Spectroscopy

4.1 Materials and Methods

X-ray absorption spectroscopy was performed at the Samba beamline of SOLEIL (Paris, France) with the storage ring operated in top-up mode (400 mA) and using a liquid-helium cryostat (samples held at 20 K) and I₀, I₁, and I₂ ion chambers for sample transmission detection and parallel measurement of the absorption of a Mo-foil serving as an energy reference (first inflection point of the K-edge at 20003.9 eV) in a standard XAS setup, as previously described.³ EXAFS data evaluation and simulation was carried out with in-house software tools.⁴

4.2 Results

Samples **1** and **1/O₂** were in acetonitrile solution, bond lengths deviations to crystal structures thus are expected. For **1**, the Mo K-edge shape, EXAFS spectrum and respective simulation parameters were in agreement with the crystal structure (Figure 1, S4 and Table 4), revealing one Mo=O bond (1.74 Å), two Mo–O bonds (1.77 Å), and pronounced contributions to the spectrum of the Mo–C interactions due to the Cp* ring, as well as two Mo–Fe distances at 3.45 Å. For **1/O₂**, the K-edge revealed an increased pre-edge feature (at 20010 eV), which suggested an increased number of Mo=O bonds. In the EXAFS spectrum, Mo–C_{Cp*} contributions were not observed. EXAFS simulations revealed a first-sphere coordination of the Mo with likely four Mo–oxygen bonds (2× 1.70 Å and 2× 1.93 Å). The presence of two molybdenum–oxygen distances differing by 0.2 Å explained the diminished FT amplitude of **1/O₂** compared to **1**, which is due to interference effects. The Mo–Fe distances in **1/O₂** seemed to be slightly shorter compared to **1**. Mo–C distances were not required to simulate the spectrum.

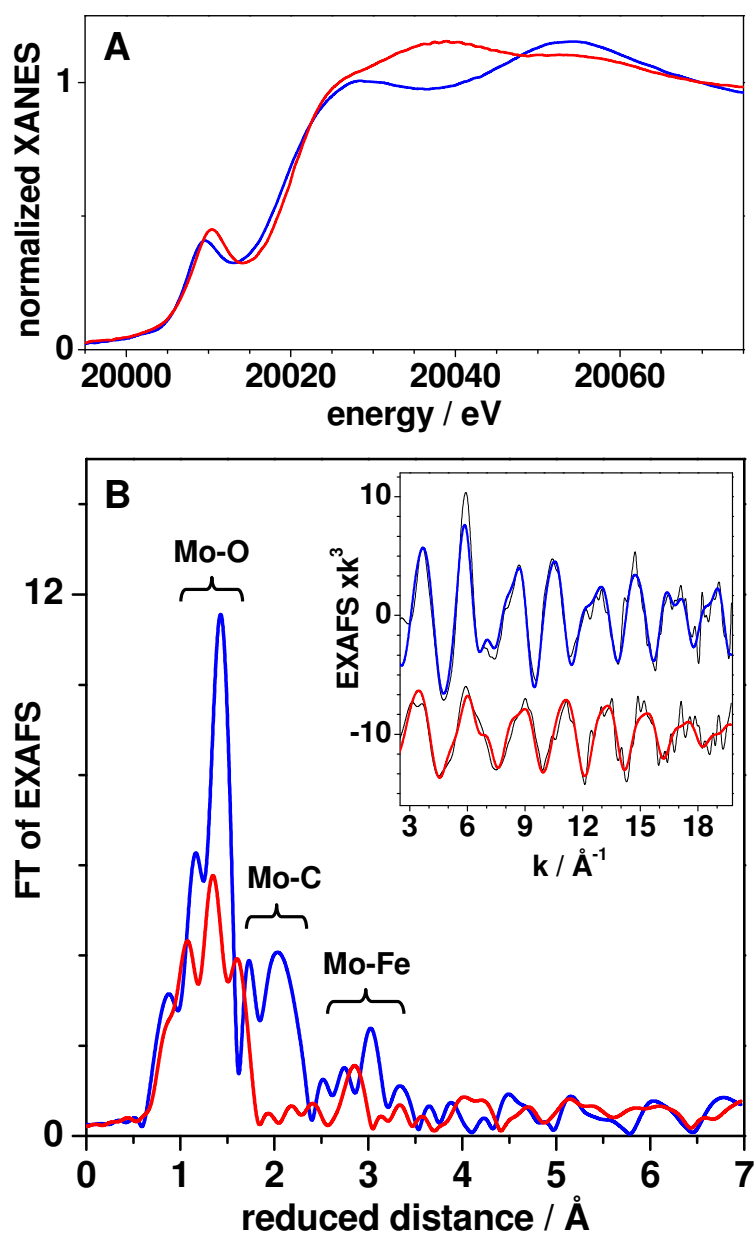


Figure S11: XAS spectra of **1**(blue) and **1**/O₂ (red). (A) Mo K-edge spectra. (B) Fourier-transforms (FTs) of experimental EXAFS spectra in the inset. Inset: coloured lines, simulations calculated with parameters in Table S4; black lines, experimental data. FTs were calculated for k-values of 2-19.8 Å⁻¹ (15-1500 eV) using cos-windows extending over 10% of both k-range ends.

5 UV/VIS Spectroscopy

5.1 UV/VIS spectrum of $[(\text{TPA})\text{Fe}(\mu-\text{Cp}^*\text{MoO}_3)]_2(\text{OTf})_2$ (1)

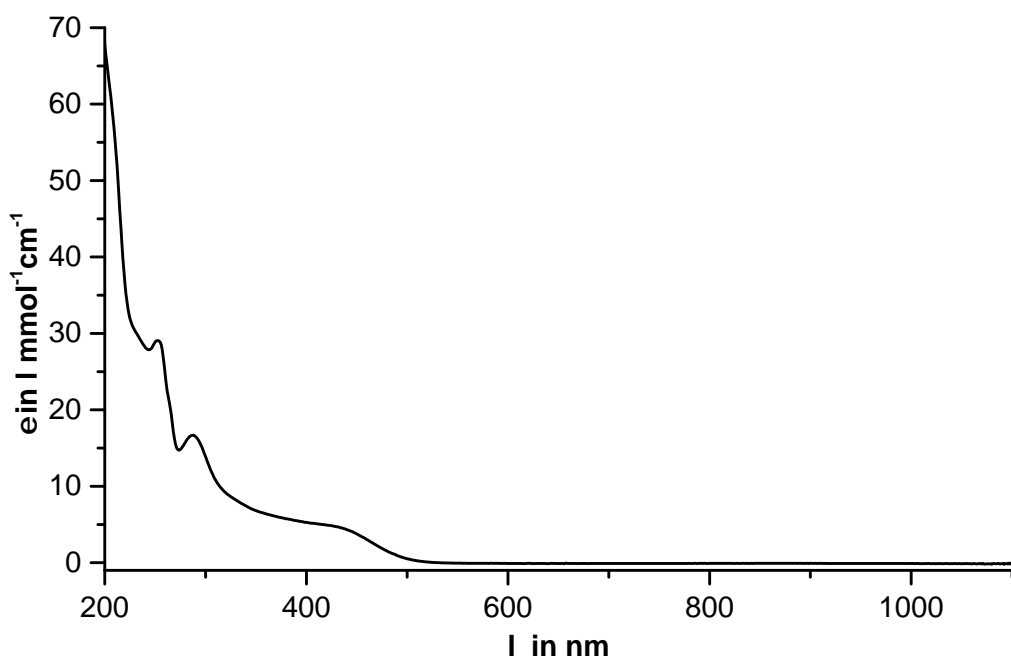


Figure S12: UV/VIS spectrum of 0.1 mM $[(\text{TPA})\text{Fe}(\mu-\text{Cp}^*\text{MoO}_3)]_2(\text{OTf})_2$ (1) measured in MeCN at 25 °C with a pathlength of 2 mm.

5.2 UV/VIS spectrum of $[(\text{TPA})\text{Fe}]_2(\mu-\text{O})(\mu-\text{MoO}_4)](\text{OTf})_2$ (2)

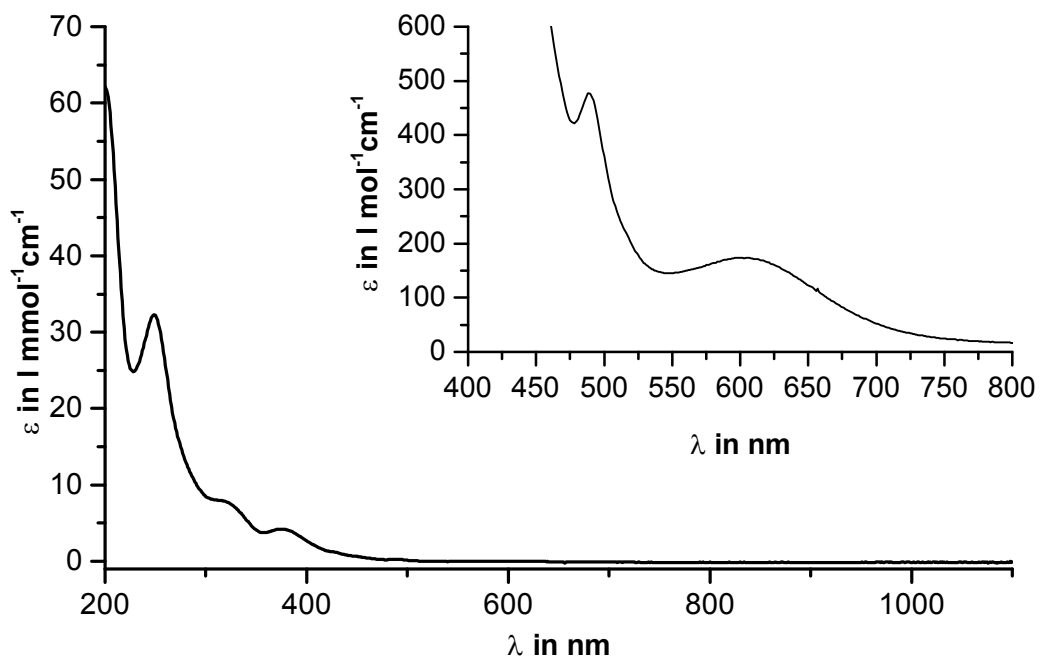


Figure S13: UV/VIS spectrum of 0.1 mM $[(\text{TPA})\text{Fe}]_2(\mu-\text{O})(\mu-\text{MoO}_4)](\text{OTf})_2$ (**2**) measured in MeCN at 25 °C with a pathlength of 2 mm. (Inset 0.5 mM, 10 mm pathlength).

5.3 UV/VIS spectrum of $[(\text{TPA})\text{Zn}(\text{Cp}^*\text{MoO}_3)]\text{OTf}$ (3)

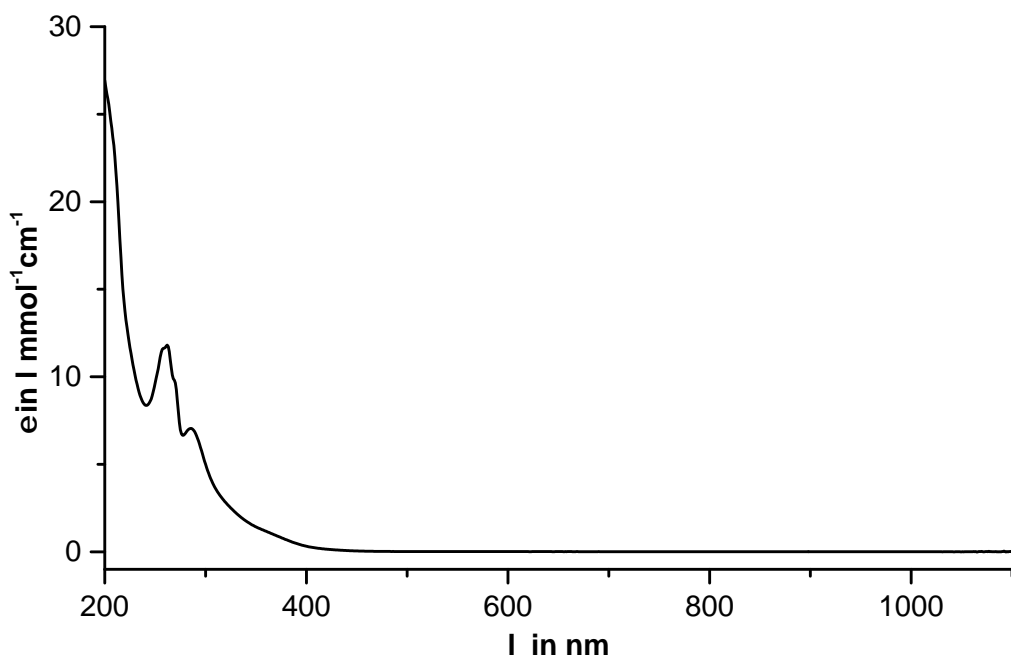


Figure S14: UV/VIS spectrum of 0.5 mM $[(\text{TPA})\text{Zn}(\text{Cp}^*\text{MoO}_3)]\text{OTf}$ (3) measured in MeCN at 25 °C with a pathlength of 2 mm.

5.4 UV/VIS spectrum of $[(\text{TPA})\text{Co}(\text{Cp}^*\text{MoO}_3)](\text{OTf})$ (4)

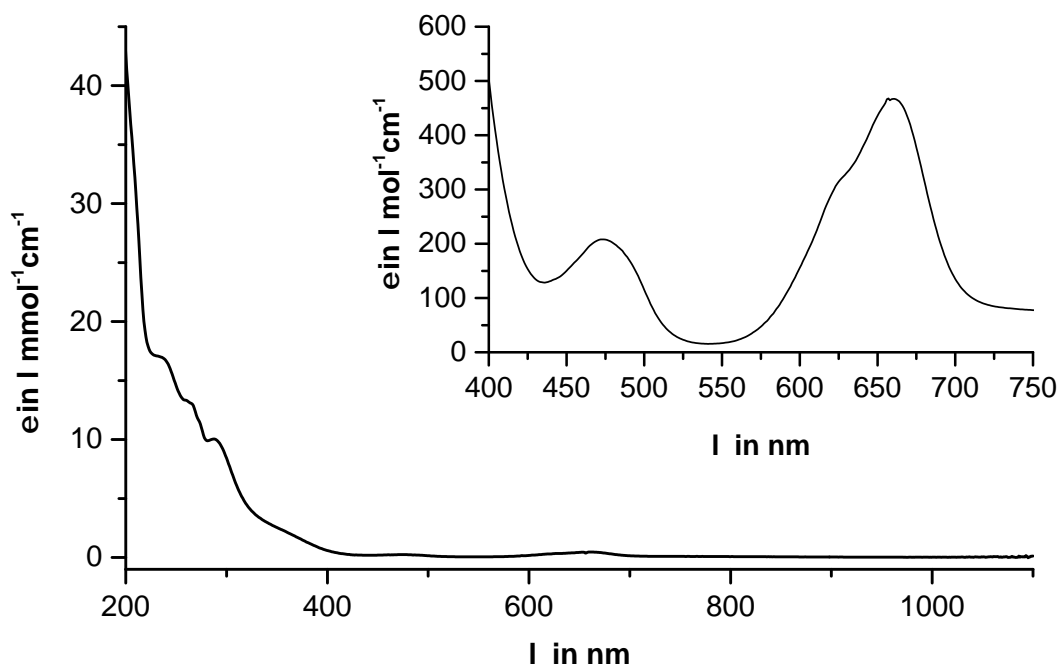


Figure S15: UV/VIS spectrum of 0.1 mM $[(\text{TPA})\text{Co}(\text{Cp}^*\text{MoO}_3)](\text{OTf})$ (4) measured in MeCN at 25 °C with a pathlength of 2 mm. (Inset 0.5 mM, 10 mm pathlength.

5.5 UV/VIS spectrum of $[(\text{TPA})\text{Co}_2(\mu-\text{Mo}_2\text{O}_8)](\text{OTf})_2$ (5)

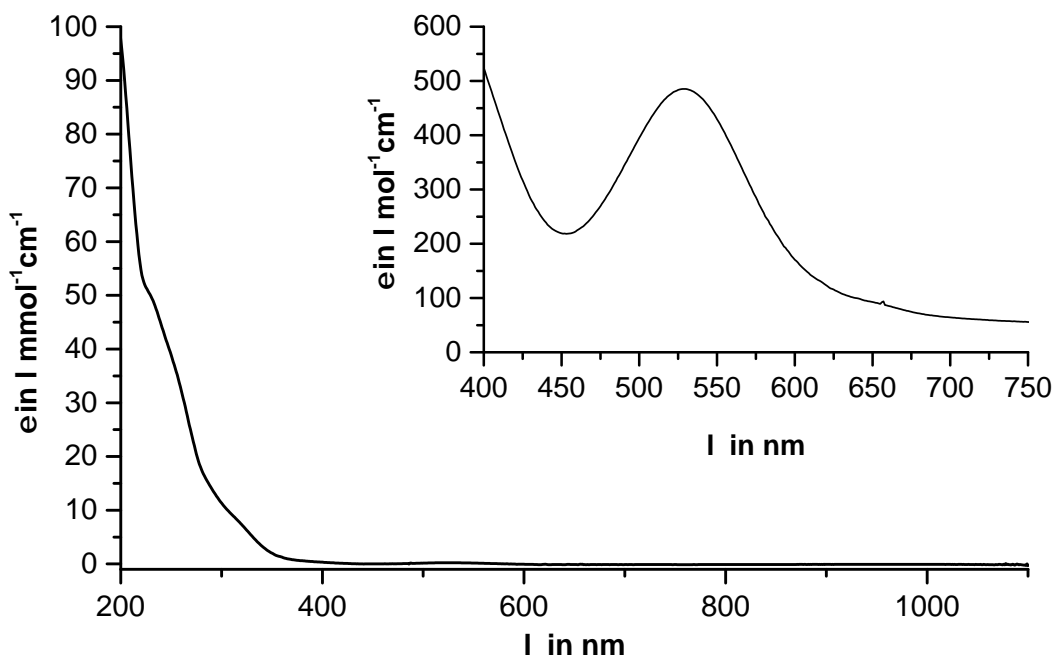


Figure S16: UV/VIS spectrum of 0.1 mM $[(\text{TPA})\text{Co}_2(\mu-\text{Mo}_2\text{O}_8)](\text{OTf})_2$ (5) measured in MeCN at 25 °C with a pathlength of 2 mm. (Inset 0.5 mM, 10 mm pathlength)

5.6 UV/VIS spectrum of $[(\text{TPA})\text{Fe}(\mu-\text{MoO}_4)]_2$ (6)

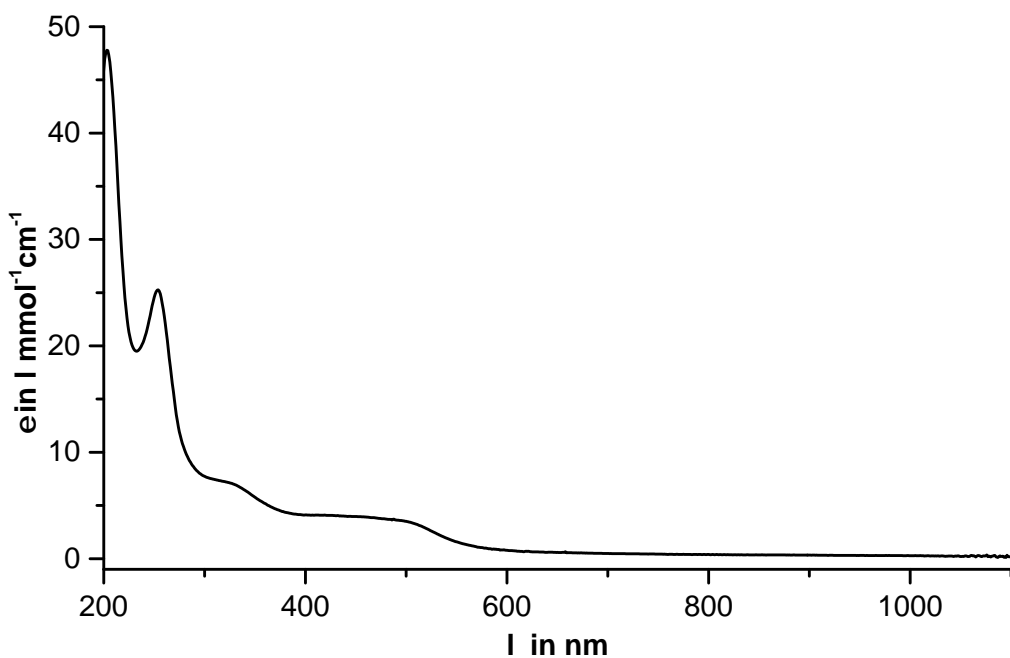


Figure S17: UV/VIS spectrum of 0.02 mM $[(\text{TPA})\text{Fe}(\mu-\text{MoO}_4)]_2$ (6) measured in MeCN at 25 °C with a pathlength of 10 mm.

6 Mößbauer Spectroscopy of $[(\text{TPA})\text{Fe}(\mu-\text{Cp}^*\text{MoO}_3)]_2(\text{OTf})_2$ (1)

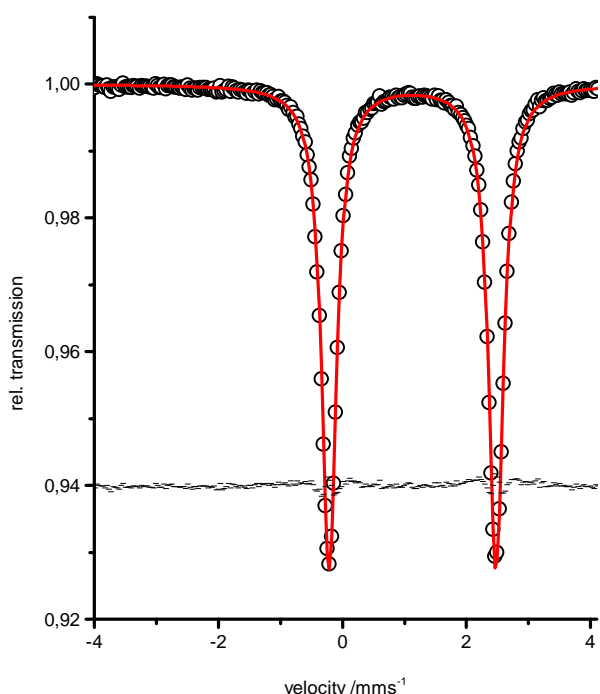


Figure S18: Mößbauer spectrum of solid **1** at 80 K. Fit parameters I.S. 1.13, Q.S. 2.69, fwhm 0.29, I_R/L , fsumsq: 0.5858E+00, Int.: 0.1975E+01, theo. Int.: 0.1976E+01 (100.02 %).

References

- [1] L. J. Ming, H. G. Jang and L. Que, *Inorg. Chem.*, 1992, **31**, 359–364.
- [2] I. Solomon, *Phys. Rev.*, 1955, **99**, 559–565.
- [3] K. G. V. Havelius, S. Reschke, S. Horn, A. Döring, D. Niks, R. Hille, C. Schulzke, S. Leimkühler and M. Haumann, *Inorg. Chem.*, 2011, **50**, 741–748.
- [4] H. Dau, P. Liebisch and M. Haumann, *Anal. Bioanal. Chem.*, 2003, **376**, 562–583.